RSC Advances

ROYAL SOCIETY OF CHEMISTRY

www.rsc.org/advances

Environmentally benign synthesis of band gap-tunable Te/Se alloyed nanowires with high-quality homogenous

Chongjian Zhou[1], Ke Wang[1], Chaochao Dun[3], Qiong Wang[1], Zhongqi Shi[1,*], Guiwu Liu[2,*] and Guanjun Qiao[1,2]

[1] State Key Laboratory for Mechanical Behavior of Materials, Xi'an Jiaotong University, Xi'an 710049, China

[2] School of Materials Science and Engineering, Jiangsu University, Zhenjiang 212013, China

[3] Center for Nanotechnology and Molecular Materials, Department of Physics, Wake Forest University, Winston-Salem NC 27109, USA

Abstract

Ultrathin trigonal Te/Se alloyed nanowires with tunable compositions and band gap were fabricated by using a nonhazardous reducing agent, ascorbic acid. The as-synthesized nanowires displayed a tunable direct band gap (3.39 to 3.78 eV) and indirect band gap (1.99 eV to 2.93 eV).

Keywords: Te/Se; ultrathin; band-gap tunable

* Correponding authors at: State Key Laboratory for Mechanical Behavior of Materials, Xi'an Jiaotong University, Xi'an 710049 , China (Z. Shi)
E-mail addresses: zhongqishi@mail.xjtu.edu.cn (Z. Shi), gwliu76@ujs.edu.cn (G. Liu)

As typical p-type semiconductors with narrow band gap and high activity in hydration and oxidation reactions, Te, Se and Te/Se alloys are excellent candidates in fields of gas sensing[1], piezoelectric[2], thermoelectric[3–7] and photoconductivity[8,9]. Te/Se alloys are composed of Te-Se atom-bonded helical chains with Te and Se atoms randomly united *via* van der Waals forces[10,11]. Both the trigonal Te (*t*-Te) and Se (*t*-Se) crystallize with space group D_3^4 that has three atoms per unit cell arranged helically along *c* axis[12], leading to almost identical properties. However, slight differences like amorphous-to-crystalline transition temperature exist, which actually results in the hard control of morphology for *t*-Te/Se alloyed nanocrystal using solution phase method[11] when it comes to the wide applications.

One commonly utilized solution-based synthesis method to fabricate metal *t*-Te/Se alloyed nanocrystal adopted hydrazine as the reducing agent[10,11,13–17], which is unfortunately explosive, pyrophoric, and carcinogenic. Hydroxylamine and sodium borohydride as alternative reducing agents are tolerable but still moderate hazardous[18–20]. Moreover, most of the reactants in previous studies involved in the expensive orthotelluric acid as Te precursor[10,13,18,21]. In contrast, ascorbic acid (Vitamin C) is believed to be a relative safe reducing agent that has been tentatively used in many solution based syntheses processes[22–24]. So far, few reports have focused on the synthesis of Te/Se alloyed nanowires using ascorbic acid as reducing agent. Moreover, as a promising thermoelectric and photoconductivity materials, band gap engineering of Te/Se nanowires is essential. However, precise control of band gap in Te/Se nanowires is difficult since band gap normally changes irregularly with the

increased Se percentage due to the poor morphology control of the alloys nanowire[11].

Herein, we put forward an environmental benign and scalable one-pot strategy to fabricate high-quality *t*-Te/Se nanowires with well controlled aspects ratio by using ascorbic acid as reducing agent. The synthesis method used Te nanowires with different aspects ratio as sacrifice template. By injecting Se precursor at certain temperature, high quality ultrathin Te/Se alloyed nanowires with diameter less than 10 nm were synthesized. Unlike previously reports[11], the as-synthesized alloyed nanowires were determined as a single phase instead of a simple core-shell structure, which exhibited a continuously tunable band gap and could be used as photoconductivity and thermoelectric materials.

Take the typical $Te_{0.5}Se_{0.5}$ nanowires with an average diameter around 10 nm as an example, the synthesis of *t*-Te/Se nanowires was accomplished as follows: (1) Synthesis of Te nanowires with an average diameter around 6 nm. 3 mmol tellurium dioxide (TeO_2), 0.75 g polyvinylpyrrolidone (PVP, M_w~40000), and 10 mmol KOH were dissolved in 30 mmol ethylene glycol (EG) with vigorous stirring that resulted in a cloudy white solution. A transparent yellow solution was obtained after heating to 120 °C. Then 6 ml 1.89 M aqueous solution of ascorbic acid was rapidly injected and the solution turned opaque black within 1 min. The reaction proceeded 3 h under N_2 protection to let the Te precursor convert to ultrathin Te nanowires. (2) Formation of Te@Se core-shell nanowires. Se precursor solution was prepared by dissolving 3 mmol selenic acid (H_2SeO_3) and 0.1 g PVP in 10 ml EG, followed by heating to ~80 °C in a separate vial. Meanwhile, the Te solution was cooled down to 90 °C. The

Se solution was injected to the Te reaction solution, and then 2.5 ml 18 M hydrochloric acid (HCl) dissolved in 2.5 ml EG was also injected to the solution to form Te@Se core-shell nanowires. (3) Transform of Te@Se core-shell nanowires to $Te_{0.5}Se_{0.5}$ alloyed nanowires. The solution temperature was raised to 110 °C for another hour, after which the reaction solution was cooled down to room temperature naturally. Finally, the $Te_{0.5}Se_{0.5}$ alloyed nanowires were successfully obtained. The Te/Se alloyed nanowires with tunable compositions can also be synthesized and their yields were higher than 90%. Similarly, by appropriate control the synthesis procedure, Te/Se nanowires with tunable aspect ratio can be fabricated by simply tuning the aspect ratio of the Te nanowires template (Figure S1). Detail experimental process and characterization can be found in the Supporting Information.

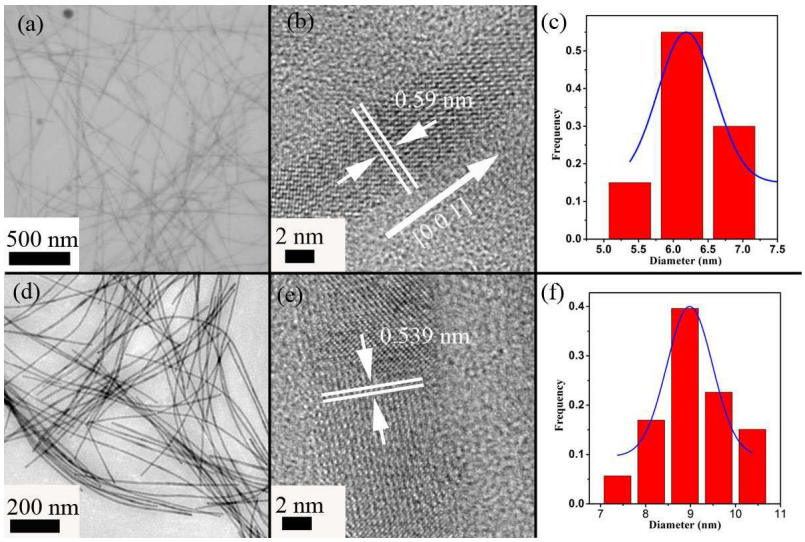

Figure 1. TEM, HRTEM images and the diameter distributions of Te nanowires (a-c) and $Te_{0.5}Se_{0.5}$ nanowires (d-f), respectively.

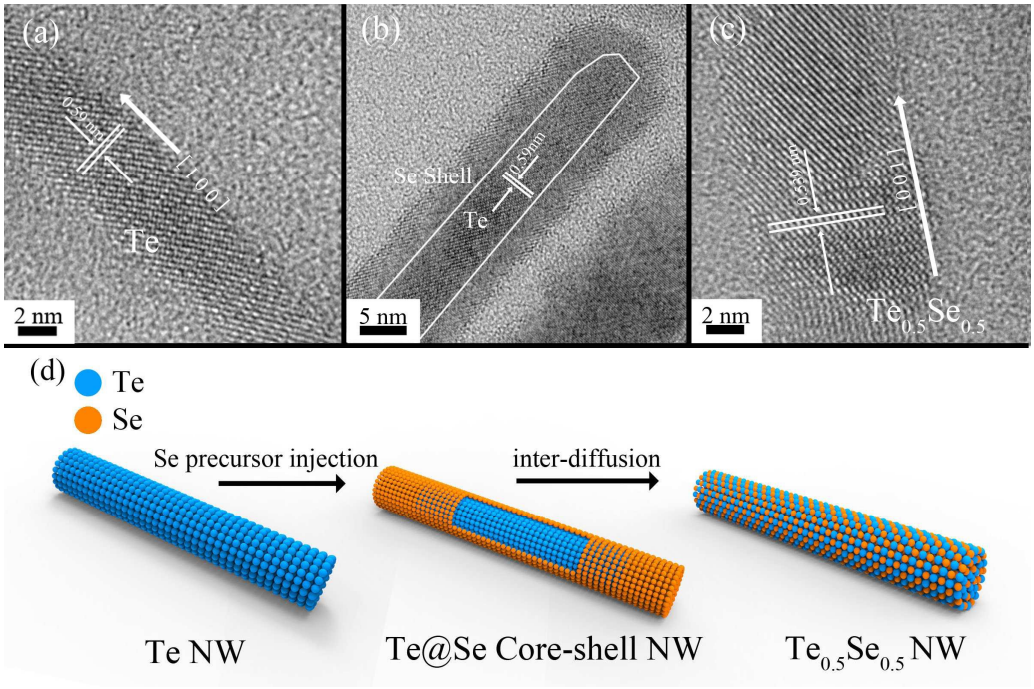

Figure 2. HRTEM of the fabricated nanowires: (a) Te nanowire (NW), (b) Te@Se core-shell structure NW, and (c) uniform single crystal $Te_{0.5}Se_{0.5}$ NW after atom inter-diffusion. (d) Schematic formation process was also displayed.

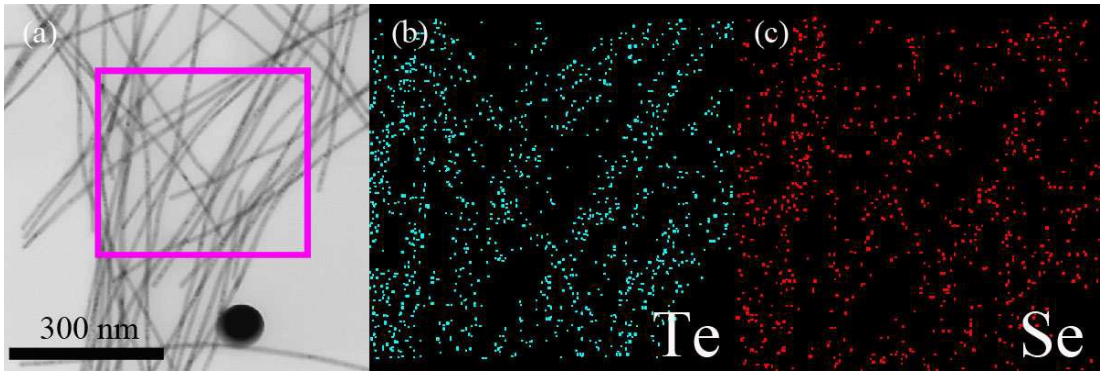

Figure 3. EDS elemental mapping of the synthesized $Te_{0.5}Se_{0.5}$ nanowires, which reveals a homogeneous distribution of Te and Se atoms with ratio 1:0.9.

Figure 1(a) and Figure 1(d) show the transmission electron microscopy (TEM) images of Te and $Te_{0.5}Se_{0.5}$ nanowires, respectively. It can be seen that both of them

distribute separately with homogeneous diameters. HRTEM image (Figure 1(b)) of an individual Te nanowire reveals the high crystallization nature and the [001] preferential lattice plane of Te, which is in agreement with the previous report[25]. As shown in Figure 1(c), the mean diameter of Te nanowires is in range of 6-7 nm, with lateral length reaching around 975±47 nm. On the other hand, the TEM and HRTEM images of $Te_{0.5}Se_{0.5}$ nanowires (Figure 1(d) and (e)) demonstrate that the nanowires preserved the morphology and the preferential growth direction [001] of the pristine Te nanowires. The single crystallization of $Te_{0.5}Se_{0.5}$ nanowires are also verified, as shown in Figure 1(e). Compared with the Te nanowires, the mean diameter of $Te_{0.5}Se_{0.5}$ nanowires slightly increases from 6~7 nm to 9~10 nm and the length reaches as high as 1502 ±82 nm. Actually, the nanowires are quite flexible, TEM images might cause certain unreliable values because deposition of nanowires onto the TEM grid is not completely attached to the surface of TEM grid, resulting in a deviation of length than the actual values. However, from the perspective of statistical, the deviation of length measurement for the nanowires under TEM grid can be neglected when a large amount of nanowires are measured. To the best of our knowledge, it is the longest and thinnest Te/Se alloy nanowires reported so far[10,11,13,18,21,26]. The diameter and length expansions are mainly coming from the epitaxy growth of Se shell outside the fabricated Te nanowires after injecting Se precursor (Figure 2(b)). Obviously, the Se shell growth around the Te nanowire is amorphous and becomes crystalline with temperature rising. As Se and Te belong to the same group, Se atoms are allowed to diffuse into the fabricated Te nanowires

along the Te/Se interface, leading to the Te/Se alloys nanowires with preserved morphology and single crystallization. The whole growth mechanism is descripted in Figure 2(d). To further confirm the fabrication process of Te/Se alloys nanowires, energy dispersive spectroscopy (EDS) elemental mapping (Figure 3) and high-angle annular dark-field (HAADF) (Figure S2) image in the selected $Te_{0.5}Se_{0.5}$ nanowires was performed. Theoretically, brightness difference would be observed under HAADF mode if Te and Se are inhomogeneously distributed. However, as can be seen in Figure S2, no brightness difference is observed, suggesting Te and Se element are indeed distributed homogenously. The stoichiometric composition of the $Te_{0.5}Se_{0.5}$ nanowires was elucidated to be around 1:0.9 (Figure S3), which matches well with the initial precursor ratio as expected.

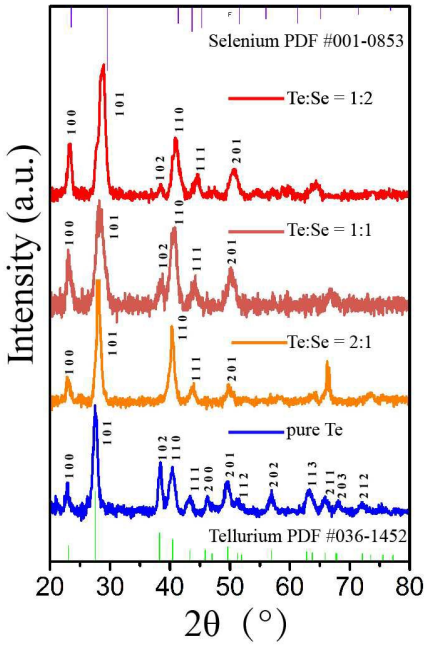

Figure 4. XRD patterns of Te nanowires and Te-Se alloyed nanowires with different composition. The corresponding standard Te (Green vertical line) and Se (Purple vertical line) patterns were also given.

In order to systematically verify the single phase of Te/Se alloys instead of a simple core-shell structure, X-ray diffraction (XRD) patterns and TEM images of the synthesized Te nanowires and Te/Se nanowires were studied, as shown in Figure 4 and Figure S4. The XRD pattern of the synthesized Te nanowires adopted as the sacrifice template matches well with that of the *t*-Te (JCPDS 36-1452). On the contrary, the peaks in the XRD pattern of Te/Se alloyed nanowires shift to a higher angle continuously compared with the Te nanowires with the increase content of Se. Here, it is apparent that the XRD pattern of Te-Se alloyed nanowire is a single phase instead of a superposition of pure Te and Se phases. From previously report, Te-Se nanowires using Te nanowires as template in water cannot get a single phase nanowire because the water was limited to a maximum reflux temperature of 100 ºC at ambient pressure[21], therefore, a mixture phase of Se_xTe_y-Te nanowires was fabricated. Here, by using EG as solvent, the synthesis temperature can be raised high enough (>110 ºC) to empower the Se atoms to diffuse uniformly into the Te nanowires. Actually, when the reaction temperature was below 110 ºC, mixture phase nanowires also existed in our product (Figure S5). With the increasing of temperature, it is believed that Se atoms were able to diffuse into the Te spiral chains until uniformly distribute in the Te/Se nanowires, as shown in Figure 2. Furthermore, from the XRD results shown in Figure 4, it was found that the diffraction peaks of $Te_{1-x}Se_x$ nanowires especially $Te_{0.5}Se_{0.5}$ are relative broaden than that of Te nanowires even the Te nanowires are thinner than their counterpart $Te_{1-x}Se_x$. This phenomenon might also be attributed to the broken of long-range atom order by the random distribution of Se atoms into Te nanowires. The

wave-like stripe pattern from the TEM dark field image of a single $Te_{0.5}Se_{0.5}$ nanowire (Figure S6) also indicates the induced stress with the inter-diffusion of Se into Te, which is believed to result from not only the high surface-to-volume ratio, but also the highly disordered distributed Se atoms along the nanowire. Actually, due to $Te_{0.5}Se_{0.5}$ nanowires possess a single phase crystallization instead of core-shell structure, no orientation contrast should be observed under dark field mode theoretically. However, the random distribution of Se and Te atoms might introduce the lattice mismatch around neighbor lattice, leading to the uneven localized force and thus the wave-like stripe patterns.

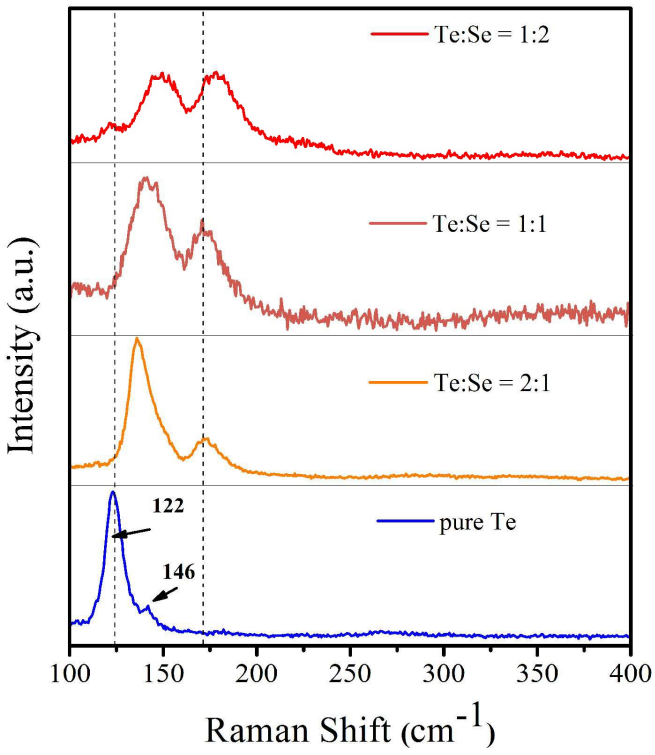

Figure 5. Raman spectra of Te/Se alloyed nanowires with different compositions.

As discussed above, the present Te/Se alloyed nanowire is a kind of pseudo-binary crystal, which means it is not only a simple mixture of Te and Se atoms,

but also exists as a pseudo-copolymer with pseudo-covalent Te-Se bonds. Raman spectroscopy was employed to quantitatively valid the intrinsic vibration property of the pseudo-binary Te/Se alloyed nanowires. As shown in Figure 5, four different compositions were investigated, i.e. Te nanowires, and Te/Se alloys nanowires with atom ratio 2:1,1:1 and 1:2. The Te nanowires present two peaks located at 122 cm^{-1} and 146 cm^{-1}, which correspond to the A_1 and E_{TO} vibration mode, respectively[27]. Obviously, the Te nanowires display a single Te-Te vibrational mode behavior. However, the Te/Se alloyed nanowires display a multi-mode vibrational behavior. For example, when Te:Se ratio is 2:1, the peak around 122 cm^{-1} seems disappear, while new peaks at 143 cm^{-1} and 174 cm^{-1} are observed. The peak at 143 cm^{-1} that corresponding to the symmetry A_2 mode is attributed to the Te-Se vibration mode which can only be found in Te-Se alloy compounds[28]. The 174 cm^{-1} is ascribed to the Se-Se vibration mode. Actually, the Te-Te mode (122 cm^{-1}) also exists, however, it is less infrared-inactive such that its intensity becomes too small to detectable[28]. The Te-Se and Se-Se modes continuously blue shift with the increase of Se percentage. However, when the ratio of Te:Se reaches 1:2, the A_1 mode of pure Te reemerged. According to the previous report[28], the reappearance of A_1 mode can be explained as the decreased intensity of Te-Se vibration mode. When the Se atom in Te/Se alloy exceed 50%, the deviated second optical band frequency that is far away from pure Te vibration also results in the reappearance of A_1 mode. Importantly, it is worth pointing out that it is the first time a transition from a single mode vibrational behavior to multi-mode vibrational behavior is observed, with continuously Raman blue shift as

Se percentage increasing in the Te/Se alloyed nanowires.

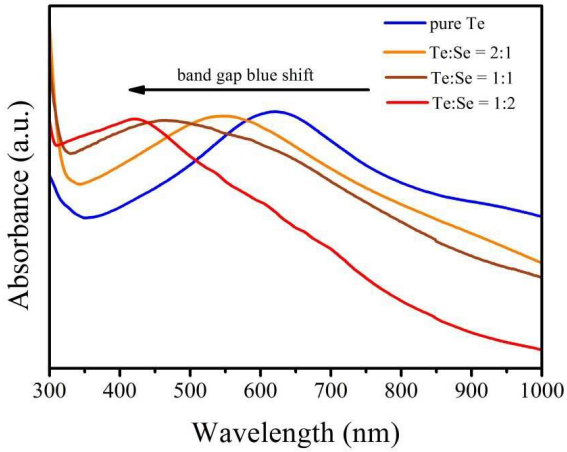

Figure 6. UV-vis absorption spectra of Te/Se alloyed nanowires with different compositions.

The UV-vis absorption spectra were performed to investigate the band gap variation of Te/Se alloyed nanowires with different compositions (Figure 6). The spectrum of Te nanowires is almost the same as the previous literature[29]. For the Te nanowires, the absorption peaks located at 365 nm (3.39 eV) and 621 nm (1.99 eV) correspond to the direct band gap and indirect band gap, respectively. With the formation of Te/Se alloyed nanowires and the increased Te:Se molar ratio, a blue shift of the UV-vis absorption spectra is clearly observed. For example, for Te:Se with molar ratio 1:2, the direct and indirect band gaps become 3.78 eV and 2.93 eV, respectively. From previous report[11], an irregular change of the band gap in Te/Se nanowires with the increased Se atom percentage was found, and the authors attributed that to the poor morphology control of the nanostructures. Here, based on the well-controlled synthesis method in our study, the synthesis of tunable compositions and continued adjustment of band gap for the ultrathin Te/Se alloy nanowires were achieved, which is critical to be used as photoconductivity and

thermoelectric materials.

In summary, a scalable and environmental benign solution-based method to synthesize homogenous and composition tunable Te/Se alloyed nanowires was proposed, which was achieved by using ascorbic acid as the reducing agent instead of the highly toxic and explosive hydrazine. The composition of Te/Se alloyed nanowires can be easily controlled by adjusting the molar ratio of TeO_2 to H_2SeO_3 during reaction. The length of the ultrathin Te/Se alloyed nanowires with tunable compositions can reach as high as 1502 nm while keeping the diameter less than 10 nm. The well controlled Te/Se alloyed nanowires also displayed a tunable direct band gap changing from 3.39 to 3.78 eV and indirect band gap changing from 1.99 eV to 2.93 eV, respectively.

These band gap tunable Te/Se nanowires are anticipated used as photoconductivity materials. Moreover, due to the nearly identical element reactivity of Te and Se, the Te/Se alloyed nanowires can also be used as an sacrifice template to synthesis other kinds of ternary nanowires, such as Cu-Te-Se, Ag-Te-Se, Pb-Te-Se and so on, all of which are promising thermoelectric materials.

Acknowledgements

This work was supported by the Program for New Century Excellent Talents in University (NCET-12-0454), Program for Young Excellent Talents in Shaanxi Province (2013KJXX-50) and the Fundamental Research Funds for the Central University (XJJ2015104)

Reference

1 Z. Wang, L. Wang, J. Huang, H. Wang, L. Pan and X. Wei, *J. Mater. Chem.*, 2010, **20**, 2457–2463.

2 T. II Lee, S. Lee, E. Lee, S. Sohn, Y. Lee, S. Lee, G. Moon, D. Kim, Y. S. Kim, J. M. Myoung and Z. L. Wang, *Adv. Mater.*, 2013, **25**, 2920–2925.

3 G. Zhang, B. Kirk, L. a Jauregui, H. Yang, X. Xu, Y. P. Chen and Y. Wu, *Nano Lett.*, 2012, **12**, 56–60.

4 K. Wang, H.-W. Liang, W.-T. Yao and S.-H. Yu, *J. Mater. Chem.*, 2011, **21**, 15057–15062.

5 C. Dun, C. Hewitt, H. Huang, D. Montgomery, J. Xu and D. Carroll, *Phys. Chem. Chem. Phys.*, 2015, **17**, 8591–8595.

6 C. Dun, C. Hewitt, H. Huang, J. Xu, D. Montgomery, W. Nie, Q. Jiang and D. L. Carroll, *ACS Appl. Mater. Interfaces*, 2015, **7**, 7054–7059.

7 F. Drymiotis, T. W. Day, D. R. Brown, N. a. Heinz and G. Jeffrey Snyder, *Appl. Phys. Lett.*, 2013, **103**, 143906.

8 B. Gates, B. Mayers, B. Cattle and Y. Xia, *Adv. Funct. Mater.*, 2002, **12**, 219–227.

9 Z.-M. Liao, C. Hou, Q. Zhao, L.-P. Liu and D.-P. Yu, *Appl. Phys. Lett.*, 2009, **95**, 093104.

10 B. B. Mayers, B. Gates, Y. Yin and Y. Xia, *Adv. Mater.*, 2001, **13**, 1380–1384.

11 S. Fu, K. Cai, L. Wu and H. Han, *CrystEngComm*, 2015, **17**, 3243–3250.

12 P. S. P.Boolchand, *Phys. Rev. B*, 1973, **7**, 57–60.

13 B. Zhou and J.-J. Zhu, *Nanotechnology*, 2006, **17**, 1763–1769.

14 D. Qin, J. Zhou, C. Luo, Y. Liu, L. Han and Y. Cao, *Nanotechnology*, 2006, **17**, 674–679.

15 H. Yang, J.-H. Bahk, T. Day, A. M. S. Mohammed, B. Min, G. J. Snyder, A. Shakouri and Y. Wu, *Nano Lett.*, 2014, **14**, 5398–5404.

16 H. Fang, H. Yang and Y. Wu, *Chem. Mater.*, 2014, **26**, 3322–3327.

17 Z. Lin, Z. Yang and H. Chang, *Cryst. Growth Des.*, 2008, **8**, 351–357.

18 G. D. Moon, Y. Min, S. Ko, S. Kim, D. Ko and U. Jeong, *ACS Nano*, 2010, **4**, 7283–7292.

19 T. J. Zhu, X. Chen, X. Y. Meng, X. B. Zhao and J. He, *Cryst. Growth Des.*, 2010, **10**, 3727–3731.

20 H. Duan, D. Wang and Y. Li, *Chem. Soc. Rev.*, 2015.

21 H. Tao, X. Shan, D. Yu, H. Liu, D. Qin and Y. Cao, *Nanoscale Res. Lett.*, 2009, **4**, 963–970.

22 N. R. Jana, L. Gearheart and C. J. Murphy, *J. Phys. Chem. B*, 2001, **105**, 4065–4067.

23 N. R. Jana, L. Gearheart and C. J. Murphy, *Adv. Mater.*, 2001, **13**, 1389–1393.

24 H. Yang, S. W. Finefrock, J. D. A. Caballero and Y. Wu, *J. Am. Chem. Soc.*, 2014, **136**, 10242–10245.

25 G. Zhang, H. Fang, H. Yang, L. A. Jauregui, Y. P. Chen and Y. Wu, *Nano Lett.*, 2012, **12**, 3627–3633.

26 K. Sridharan and T. J. P. Muhamed Shafi Ollakkan, Reji Philip, *Carbon N. Y.*, 2013, **63**, 263–273.

27 G. D. A.S.Pine, *Phys. Rev. B*, 1970, **4**, 356–371.

28 R. Geick, E. F. Steigmeier and H. Auderset, *Phys. Status Solidi*, 1972, **54**, 623–630.

29 J.-M. Song, J.-H. Zhu and S.-H. Yu, *J. Phys. Chem. B*, 2006, **110**, 23790–23795.